Journal of Power Sources 183 (2008) 92–97

Contents lists available at ScienceDirect

Journal of Power Sources

journal homepage: www.elsevier.com/locate/jpowsour

Hydrogenation and dehydrogenation of Mg_2Co nanoparticles and carbon nanotube composites

Chien-Te Hsieh*, Jin-Long Wei, Jia-Yi Lin, Wei-Yu Chen

Department of Chemical Engineering and Materials Science, Yuan Ze Fuel Cell Center, Yuan Ze University, Taoyuan 320, Taiwan, ROC

ARTICLE INFO

Article history:
Received 4 March 2008
Received in revised form 18 April 2008
Accepted 18 April 2008
Available online 3 May 2008

Keywords:
Mg-based metal hydride
Carbon nanotubes
Hydrogen storage
Dehydrogenation
Nanocomposites

ABSTRACT

This study investigated the hydrogenation and dehydrogenation behavior of Mg_2Co nanoparticles and carbon nanotube (CNT) composites using temperature-programmed deposition, Raman spectroscopy, and X-ray diffraction (XRD). We used the mechanical alloying method to prepare nanosized Mg_2Co particles on CNTs with three loadings of alloys. The introduction of CNTs showed dehydrogenation, hydrogen desorption starting at 370 °C, with the majority of hydrogen being below 500 °C. This can be explained by the fact that Mg_2Co alloy deposited on CNT surface induced the dissociation of hydrogen into two atoms, which were spilt over and then intercalated into the interlayer of CNT. Accordingly, the atomic intercalation enabled the reduction of the hydrogen desorption activation barrier. The spillover mechanism of hydrogen storage can be confirmed by XRD and Raman spectroscopy because of larger interspacing (d_{002}) and weaker graphite degree (I_D/I_G) of CNTs after hydrogenation.

1. Introduction

Hydrogen is considered as the ideal means of energy storage, transport, and conversion of energy in a comprehensive clean energy concept [1–3]. It is generally recognized that hydrogen fuel, which can be obtained from renewable energy sources, contains larger chemical energy per mass (ca. 142 MJ kg^{-1}) [4] than any other hydrocarbon fuel. Traditional approaches to hydrogen storage have focused on either physical storage of compressed hydrogen or storage in reversible metal hydrides [5]. In comparison, hydrogen storage in the solid state offers a safer alternative compared with storage in a compressed gas or liquid state. Also, storing hydrogen in metal hydrides efficiently reduces storage volume, but the metallic elements and alanates significantly increase the weight. Accordingly, some chemical hydrides, based on lithium (Li), sodium (Na), and magnesium (Mg) as light elements, have been considered as promising materials for hydrogen storage [6,7].

The practical use of hydrogen required a hydrogen storage capacity of 6 wt%, which challenges current research findings on solid-state hydrogen storage materials [8]. A few solid-state materials such as Mg and Li_3N are capable of adsorbing up to 6 wt% hydrogen [1]. However, full decomposition of hydrogen from the metal hydrides usually occurs at high temperatures. For instance, the gas evolution in $LiBH_4$ starts at 380 °C and only releases half of the hydrogen below 600 °C [9]. This drawback would limit the widespread use of metal hydrides. Thus, the main challenge in this field is to develop materials with high hydrogen sorption capacity at low temperature and ambient pressure. This development is crucial to practical hydrogen fuel cell applications.

This study intends to lower the dehydrogenation temperature of hydrogen storage materials. More recently, a pioneer study has reported that $LiBH_4$ may be reversibly dehydrogenated and rehydrogenated with a reduced reaction enthalpy by the addition of other metals [10] or carbon [9]. This addition is believed to destabilize the $LiBH_4$, resulting in complete dehydrogenation, thus leading to a lower hydrogenation/dehydrogenation temperature. The above deduction directs us into a new concept: a novel hydrogen storage nanocomposite. The addition of transition metal or carbon enables destabilization of the metal hydride (thermodynamic problem) and the nanostructure allows easy hydrogen transport (kinetic problem). Here we report an efficient approach to synthesize bimetallic Mg_2Co nanoparticles and carbon nanotube (CNT) composites. To our knowledge, the role that incorporation of MgCo alloy with CNTs plays in enhancing hydrogenation/dehydrogenation performance has not yet been clearly elucidated. We aimed to investigate the effect of Mg_2Co loading amount on the hydrogenation/dehydrogenation of the resulting composites.

2. Experimental

A procedure of mechanical alloying for preparing hydrogen storage nanocomposites was described as follows. The multiwalled

* Corresponding author. Tel.: +886 3 4638800x2577; fax: +886 3 4559373.
E-mail address: cthsieh@saturn.yzu.edu.tw (C.-T. Hsieh).

0378-7753/$ – see front matter © 2008 Elsevier B.V. All rights reserved.
doi:10.1016/j.jpowsour.2008.04.057

CNTs used in this work were prepared by a catalytic chemical vapor deposition technique, using ethylene and Ni particle as carbon precursor and catalyst, respectively. A 2:1 atomic ratio mixture of Mg and Co powders was first milled in a high-performance 3D mixer/mill (Spex 8000) for 10 h. The 2Mg–Co powder and ZrO_2 balls were placed in a container (weight ratio of ZrO_2:2Mg–Co = 5:1), filled with high-purity Ar gas. This pre-milling process enabled the grinding of the powders from micrometer to submicrometer level. Afterward, the CNT sample was added into the container and then milled up to a total time of 20 h. At this time, the ZrO_2 ball to 2Mg–Co/CNT composite weight ratio was raised to 40:1; three weight ratios of 2Mg–Co to CNT were set at 1:9, 2:8, and 3:7. To avoid any oxygen contamination, this container was refilled with Ar gas repeatedly during the mechanical alloying process.

Prior to hydrogenation, all prepared composites were cleaned under vacuum (approximately 10^{-5} mm Hg) at 350 °C. Then, the 2Mg–Co/CNT composites were hydrogenated in a high-pressure tank under 10 MPa hydrogen pressure at 120 °C for 12 h. Hydrogen release measurements were confirmed by the temperature-programmed desorption (TPD), using differential thermal analysis/thermogravimetry (TG, TG-7, PerkinElmer) with a heating rate of 5 °C min^{-1} under 1 atm argon with a purge rate of 200 cm^3 min^{-1}. The TPD analysis of H_2 was conducted in the temperature range of 30–600 °C. The sample quantities of 2Mg–Co/CNT composites were approximately 20–30 mg, which were sufficient to obtain accurate results because of the highly sensitive equipment used.

The crystalline structure of 2Mg–Co/CNT composites was characterized by Raman spectroscopy (Renishaw Micro-Raman spectrometer) and X-ray diffraction (XRD) with Cu Kα radiation using an automated X-ray diffractometer (Shimazu Labx XRD-6000). The deposition of Mg_2Co on CNTs was studied by scanning electron microscopy (SEM, Jeol 2010). Specific surface areas and pore volumes of the derived nanocomposites were determined by N_2 adsorption. An automated adsorption apparatus (Micromeritics, ASAP 2000) was used for these measurements. Adsorption of N_2 was performed at −196 °C. Nitrogen surface areas and micropore volumes of the samples were determined from the Brunauer–Emmett–Teller (BET) and Dubinin–Radushkevich (D–R) equations, respectively. The amount of N_2 adsorbed at relative pressures near unity (p/p_0 = 0.98 in this work) has been used to determine the total pore volume, which corresponds to the sum of the micropore and mesopore volumes.

3. Results and discussion

Fig. 1(a) and (b) show SEM images for Mg_2Co nanoparticles deposited on CNTs at low and high magnification, respectively. It can be observed from these images that aggregation of the alloy nanoparticles was not obvious, and that the Mg_2Co nanoparticles were highly dispersed on the CNTs. The nanotubes were found to have diameter distribution between 30 and 80 nm. Almost all alloy particles are coated on CNT surface, and particle sizes for all CNT samples were found within a constant range, 20–30 nm. The deposition of uniformly dispersed nanoalloys on CNTs is assumed to be the result of high-performance mechanical alloying.

Fig. 2 depicts the typical isotherms of N_2 adsorption/desorption onto the H_2 storage composites. The isotherms exhibited obvious hysteresis behavior at high relative pressure, showing that the composites are mainly mesoporous. The surface characteristics of the Mg_2Co–CNT composites, calculated according to the adsorption data, are summarized in Table 1. To clarify the composites, these samples were designated as MgCo–CNT, followed by the order of alloy loadings. In comparison with fresh CNTs, the Mg_2Co–CNT composites showed a decrease in specific surface area and porosity. This porosity reduction can be attributed to the fact that both ends of the nanotubes are possibly hindered by alloy aggregation, thus reducing some available porosity for the adsorption of N_2. This table also reveals that their pore size distribution showed a very slight change for all composites, indicating that the alloy loading does not destroy tube morphology after mechanical alloying.

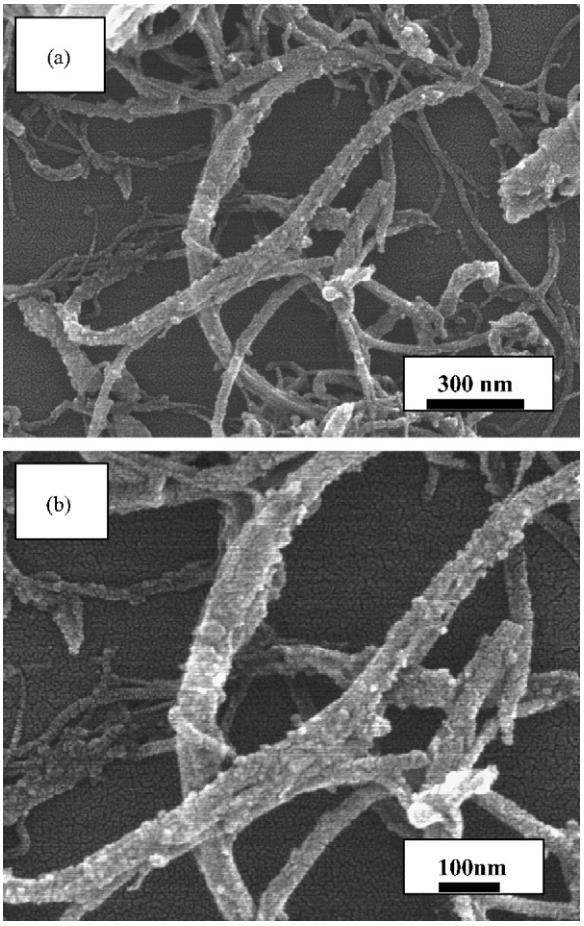

Fig. 1. SEM images of Mg_2Co nanoparticles deposited on CNTs at (a) low and (b) high magnification.

The TG profiles in Fig. 3 show hydrogen desorption properties of the Mg_2Co–CNTs prepared by mechanical alloying. All TG profiles in Fig. 3 have been subtracted from the TG curve of original CNTs, indicating correctness of weight loss contributed from hydrogen desorption. In the case of MgCo/CNT composites, the initial temperature of hydrogen desorption decreased from 415 to 370 °C. Two important observations are worth noting: (i) the onset temperature of hydrogen desorption from the hydrogenated composites was significantly affected by the additional amount of CNTs, and (ii) the total weight loss had the following order: MgCo–CNT-3 (7.1 wt%) > MgCo–CNT-2 (5.5 wt%) > MgCo–CNT-1 (3.2 wt%). Fig. 3 also apparently shows that the dehydrogenation properties of the MgCo/CNT composites have been significantly improved.

Fig. 4 shows temperature scans for the hydrogenation MgCo/CNT composites. For comparison, the TG profile of pure CNT and Mg_2Co alloy is also given (see top, Fig. 4a). Pure CNT showed an obvious evolution peak concentrated at 340–370 °C, while the H_2-desorption of Mg_2Co hydride alloy started at 620 °C and concentrated at 635 °C. In comparison with pure CNT and Mg_2Co, MgCo/CNT composites apparently generated a different H_2-desorption behavior, i.e., lower desorption temperature and two

Table 1
Surface characteristics of fresh and alloy-coated CNTs determined from nitrogen physisorption at −196 °C

Material type	Mg_2Co/CNT ratio (wt%)	S_{BET}[a] ($m^2\ g^{-1}$)	V_t[b] ($cm^3\ g^{-1}$)	Pore size distribution	
				V_{micro}[c] (%)	V_{meso}[d] (%)
Fresh CNT	0	225	0.726	9	91
MgCo–CNT-1	10	167	0.703	9	91
MgCo–CNT-2	20	176	0.558	4	96
MgCo–CNT-3	30	166	0.510	5	95

[a] S_{BET}: specific surface area computed using BET equation.
[b] V_t: total pore volume estimated at a relative pressure of 0.98.
[c] V_{micro}: micropore volume determined from the DR equation.
[d] V_{meso}: mesopore volume determined from the subtraction of micropore volume from total pore volume.

evolution peaks. The TPD analysis revealed that, when the hydrogenated composites were heated, H_2 gas evolution took place in two main stages, indicating two kinds of adsorbed H_2 in the MgCo/CNT composites. A comparison of the two peaks with pure Mg_2Co data suggests that the MgCo/CNT composites have a new intercalation compound. Additionally, these H_2 desorption curves also show that the presence of CNTs could lower the dehydrogenation temperature at both desorption stages. This can be inferred by the fact that both maximal evolution rates were shifted to lower desorption temperatures. An optimal ratio of CNTs would destabilize the hydrogenation of the MgCo/CNT composites, thus inducing the reversibility of the H_2 adsorption/desorption.

Based on this deduction, the hydrogen storage mechanism in the MgCo/CNT composites can be tentatively expressed as

$$H_2 + Mg_2Co \leftrightarrow [Mg_2CO \cdot H_2]^*_{ads} \quad (R1)$$

$$[Mg_2Co \cdot H_2]^*_{ads} + CNT \leftrightarrow CNT \cdot 2H_{ads} + Mg_2Co \quad (R2)$$

Each nanosized Mg_2Co particle first adsorbs hydrogen molecules, forming an adsorbed intermediate $[Mg_2Co \cdot H_2]^*_{ads}$. This implies that high coverage of bimetallic alloy particles would promote hydrogen storage capability. Since the Mg_2Co intermetallic compound is an unstable form, part of the alloy would be the more stable Mg_2CoH_5 [11,12]. Here, the appearance of Co plays two important roles in catalyzing one H_2 molecule adsorbed on the Mg_2Co surface forming two H atoms and in expediting the dehydrogenation of Mg_2CoH_5, thus regenerating the Mg_2Co surface for the next adsorption of hydrogen molecules. It is generally recognized that transition metals enable the hydrogen dissociation on the CNT surface [13]. In (R2), the dissociated hydrogen atoms are spilt over the multilayered CNTs, as described in the literature [14–16]. Since the CNTs have well-defined graphite layers (i.e., sp^2 structure), H atoms are believed to be thermodynamically unstable upon insertion into the interlayer of the multiwalled CNTs [4]. The other possible way to achieve atomic hydrogen storage is through dangling bonding for strong interaction between H atoms and the defects on both ends of CNTs [17].

This schematic diagram for the H_2 storage mechanism is illustrated in Fig. 5. The spillover mechanism consists of hydrogen dissociation on alloy surface, atomic diffusion, and intercalation in nanotubes. The nanosized Mg_2Co alloy is proposed to help achieve fast diffusion needed for spillover of hydrogen atoms. The CNTs act as an acceptor, providing an excessive number of active sites for atomic intercalation or adsorption. It is generally recognized that atomic insertion into the interlayer of CNTs has a lower enthalpy than the formation of hydrides. The presence of CNTs would facilitate destabilizing the decomposition of hydrides or hydrogenated composites, leading to a lower dehydrogenation temperature.

The variations of evolution temperature and weight loss with cycle number are illustrated in Fig. 6. We find that H_2 desorption capacity rapidly decreases within first three cycles and then gradually reaches an equilibrium state, ~3.92 wt%. However, the maximal evolution temperature shows a decrease with cycle number. After 5 cycles, the evolution temperature almost keeps constant value ~320 °C. This demonstrates that the Mg_2Co/CNT composite requires formation process (at least three cycles) to stabilize the desorption behavior. Data from Fig. 6, the higher capacity of MgCo–CNT-3 (>5 wt%) appears at first three cycles. Meanwhile, the storage behavior can be attributed from the spillover mechanism. Well dispersion of transition metal enables the hydrogen dissociation on CNT surface, and then the dissociated hydrogen atoms are spilt over the multiwalled CNTs. Without catalysis of transition metal, the hydrogen molecules merely adsorbed on some specific sites of CNTs, such as structural defects, functional groups or dangling bonds, that is, chemisorption. This results in a low hydrogen storage capacity. As show in Fig. 3, the TG of pure CNT has only about 2 wt% capacity.

With increasing the cycle number, the Mg_2Co/CNT composite maintains the stable capacity ~3.92 wt%, which is much lower than 7.1 wt% at initial stage. This capacity decline can be explained by two possible reasons: (i) transition metal gradually lost its catalysis capability after cycling due to occupancy or poisoning of some gaseous molecules (e.g. CO from CNT surface), and (ii) dramatic volume change of alloy after hydrogenation/dehydrogenation cycling would result in isolation or separation of alloy particles from CNT surface, thus hindering the pathway of H-atoms form alloy particle to CNT.

To identify the crystalline transformation before and after hydrogenation, XRD analysis was applied to examine the MgCo/CNT composites. The XRD patterns for MgCo–CNT-3 sample are shown in Fig. 7. Before hydrogenation, the XRD pattern clearly showed typical peaks of Mg, Co, and C appearing in the composite, prepared by mechanical alloying. No other diffraction peaks of new phases such as MgO were found. However, after hydrogen adsorption, an obvious diffraction peak corresponding to Mg_2CoH_5 occurred at the scattering angle ~62°. This can be attributed to the fact that part of Mg_2Co alloy has been hydrogenated. According to the above mechanism, we can infer that a major part of the hydrogen was dispersed in an atomic scale and formed an intercalation compound.

It is well known that the peak at ca. $2\theta = 26°$ corresponds to a graphite, which is attributed to the graphitic structure of CNTs in our case. The interlayer distance, d_{002}, of CNT crystalline can be obtained by Bragg's equation. Table 2 shows the calculated d_{002} values for all MgCo/CNT composites before and after hydrogenation. Before hydrogenation, the d_{002} values of MgCo/CNT composites (ca. 3.441–3.448 Å) gave an interlayer space close to that of a highly oriented graphite carbon (3.350 Å) [18]. In comparison with the composites before hydrogenation, the MgCo/CNT composites after hydrogenation showed larger values of d_{002}, ranging from 3.459 to 3.521 Å. The larger interspacing of the graphite layer was presumably due to the atomic intercalation. This intercalation behavior induced the reduction of the hydrogen desorption activation barrier since the inserted H atom was energetically unstable upon insertions into the interlayer of multiwalled CNTs, thus lowering

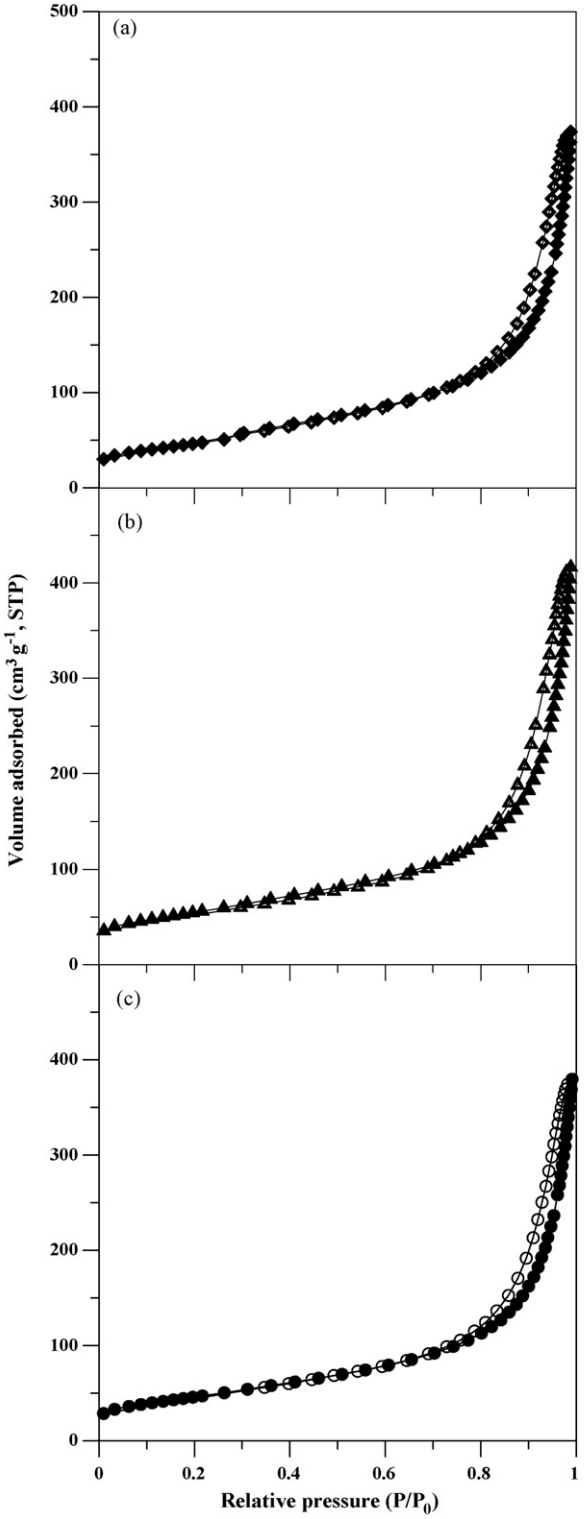

Fig. 2. Nitrogen adsorption and desorption isotherms of Mg_2Co/CNT composites: (a) MgCo–CNT-1, (b) MgCo–CNT-2, and (c) MgCo–CNT-3.

the desorption temperature. Previous studies also pointed out that hydrogen could stay in the interlayer space of the graphite of multilayered CNT [8,19,20]. In addition, it is worth noting that the d_{002} value gradually increased with Mg_2Co loading. This can be attributed to the fact that the high coverage of Mg_2Co alloy provided more adsorptive sites for adsorbing H_2 molecules. Then the

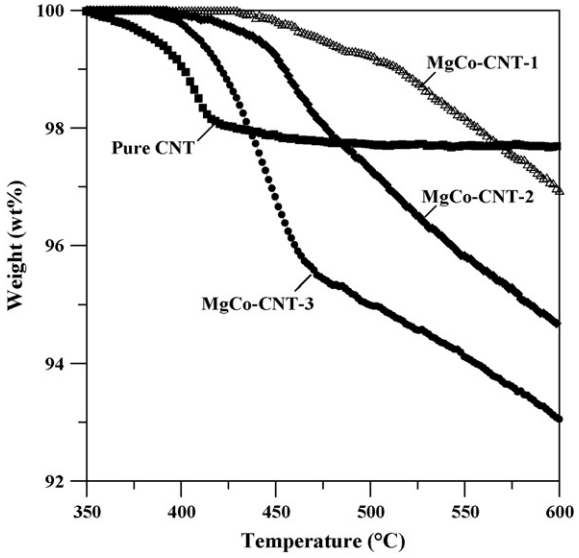

Fig. 3. TG profiles of different Mg_2Co/CNT composites at a heating rate of 5 °C min^{-1} under Ar atmosphere.

adsorbed hydrogen molecules were dissociated into two atoms, which were spilt over and intercalated into the interlayer of CNTs. The atomic intercalation resulted in a large value of d_{002}. This finding is in agreement with our spillover mechanism of hydrogen storage.

The Raman spectra of the MgCo/CNT composites before and after hydrogenation are shown in Fig. 8. The Raman band observed at 1580 cm^{-1} was assigned to a single crystallite of graphite (G band),

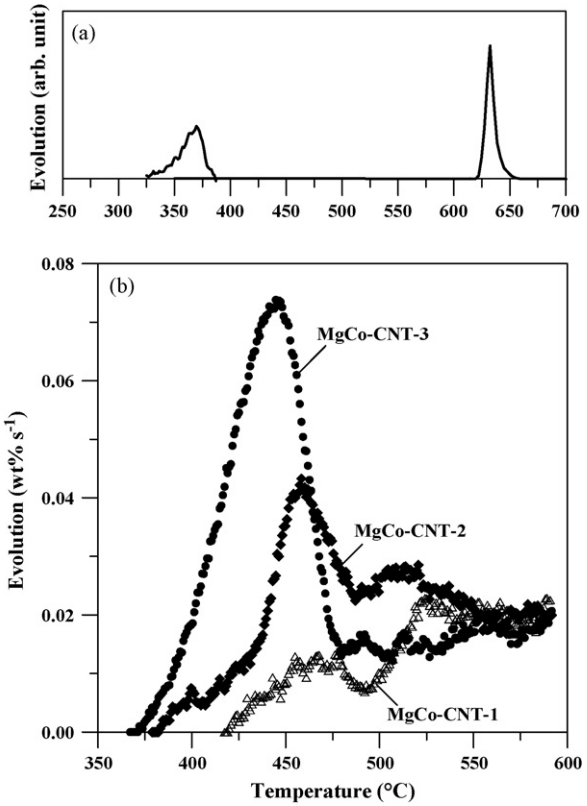

Fig. 4. TPD profile of (a) pure CNT and Mg_2Co and (b) different types of Mg_2Co/CNT composites at a heating rate of 5 °C min^{-1} under Ar atmosphere.

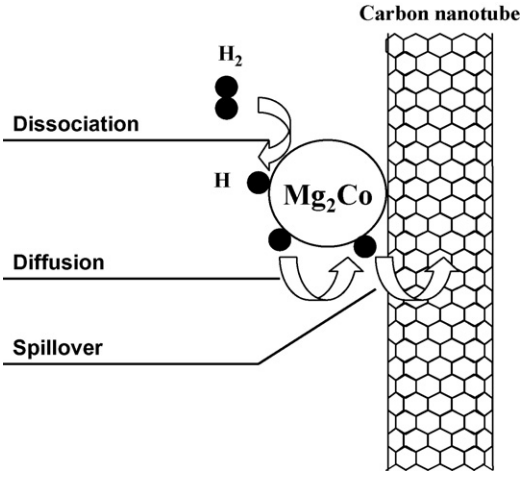

Fig. 5. Illustration for spillover mechanism of hydrogen storage on Mg_2Co/CNT composite, consisting of three steps: dissociation, diffusion, and spillover.

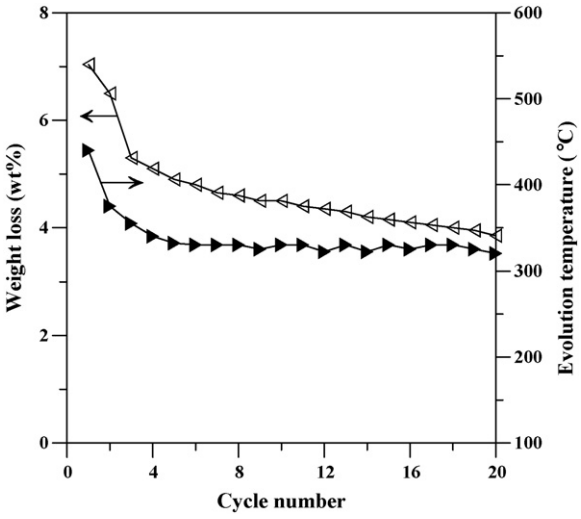

Fig. 6. Variations of weight loss and maximal H_2-evoluted temperature on MgCo–CNT-3 composite with cycle number.

whereas the additional band at 1340 cm^{-1} was attributed to amorphous carbon or deformation vibrations of a hexagonal ring (D band) [16,17,21]. It is known that the intensity ratio of the intensities of the D and G peaks (I_D/I_G) gives information on the graphite degree of carbon-based materials. From Fig. 8 data, the I_D/I_G ratios are shown in Table 2. For the MgCo–CNT-3 sample, the I_D/I_G ratio was found to increase from 0.860 (before hydrogenation) to 0.885 (after hydrogenation). This increase in I_D/I_G ratio reflects the low graphite degree or the creation of defects at CNTs after hydrogenation. Again, this result can be ascribed to the appearance of a new intercalation compound in the MgCo/CNT composite.

Table 2
XRD and Raman spectra analyses on fresh and alloy-coated CNTs before and after hydrogen storage

CNT type	d_{002} (Å)	I_D/I_G
Before hydrogenation		
MgCo–CNT-1	3.448	0.768
MgCo–CNT-2	3.441	0.842
MgCo–CNT-3	3.445	0.859
After hydrogenation		
MgCo–CNT-1	3.459	0.798
MgCo–CNT-2	3.510	0.852
MgCo–CNT-3	3.521	0.886

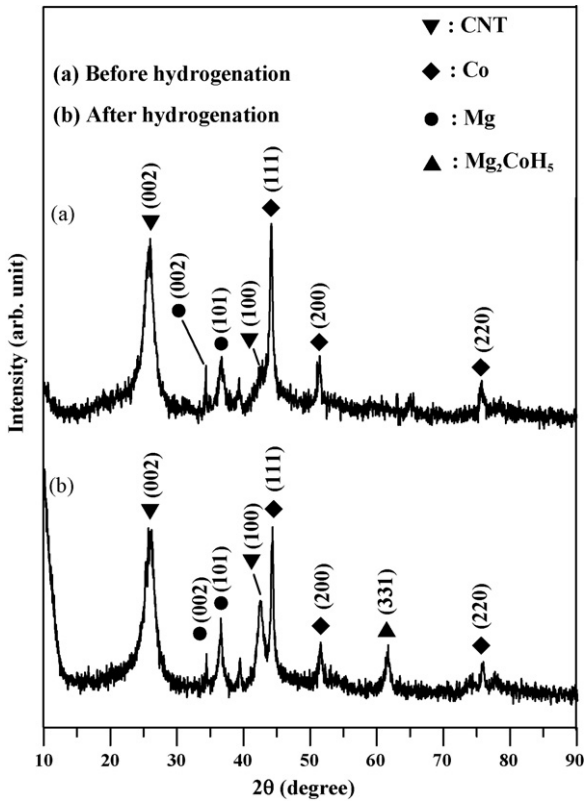

Fig. 7. X-ray diffraction pattern of MgCo–CNT-3 sample before and after hydrogenation.

Moreover, increasing the Mg_2Co loading results in the increase of the degree of disorder of CNTs, as shown in Table 2. This can also be attributed to the fact that high surface coverage of Mg_2Co alloy deposited on CNTs promotes the atomic spillover into CNTs, leading to a large number of intercalated H atoms. The larger the amount

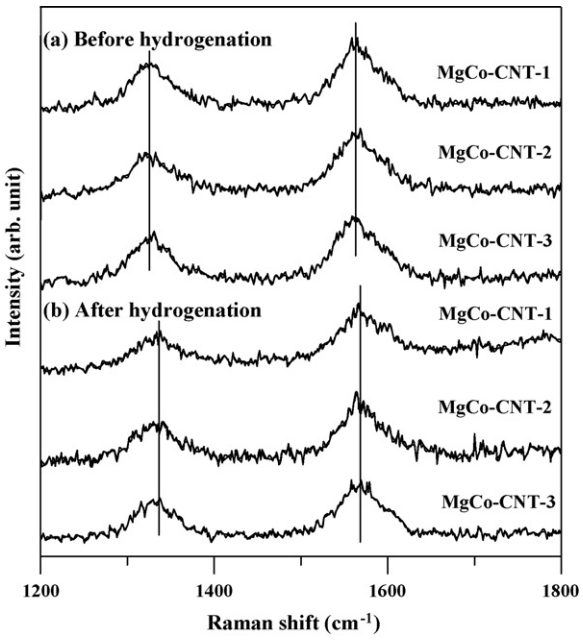

Fig. 8. Raman spectra of Mg_2Co/CNT composites before and after hydrogenation.

of atomic intercalation is, the lower the graphite degree of CNTs is obtained. The MgCo-coated CNT is considered a novel nanostructure capable of enhancing hydrogen storage performance, i.e., low dehydrogenation temperature, reversibility of H_2-storage, adsorption kinetic, and H_2-storage capacity at room temperature.

4. Conclusions

Hydrogenation and dehydrogenation of bimetallic Mg_2Co alloy deposited on CNTs were investigated using the TPD technique within the temperature region of 50–600 °C. Mechanical alloying is used to prepare different alloy loadings onto CNTs, forming the H_2 storage nanocomposites. The TPD results indicate that the presence of CNTs tends to destabilize the hydrogenation of the Mg_2Co/CNT composites, thus lowering the desorption temperature to only 370 °C. This can be attributed to the fact that Mg_2Co alloy deposited on the CNT surface induces the dissociation of H_2 into atomic hydrogen, which is spilt over and then intercalated into the interlayer of CNT. Accordingly, the atomic intercalation enables the reduction of the hydrogen desorption activation barrier because the inserted H atom is energetically unstable upon insertion into the interlayer of CNT. The spillover mechanism of hydrogen storage can be confirmed by XRD and Raman spectroscopy because of larger interspacing (d_{002}) and weaker graphite degree (I_D/I_G) of CNTs after hydrogenation.

Acknowledgment

The authors are very grateful for the financial support from the National Science Council of the Republic of China under the contract NSC 96-2221-E-155-055-MY2.

References

[1] X.L. Wang, J.P. Tu, Appl. Phys. Lett. 89 (2006) 1–3, 064101.
[2] H. Pan, Y.P. Feng, Appl. Phys. Lett. 90 (2007) 1–3, 223104.
[3] I.G. Fernández, G.O. Meyer, F.C. Gernnari, J. Alloys Compd. (2008).
[4] J.W. Lee, H.S. Kim, J.Y. Lee, J.K. Kang, Appl. Phys. Lett. 88 (2006) 1–3, 143126.
[5] A.J. Williamson, F.A. Reboredo, G. Galli, Appl. Phys. Lett. 85 (2004) 2917–2919.
[6] C.W. Hsu, S.L. Lee, R.R. Jeng, J.C. Lin, Int. J. Hydrogen Energy 32 (2007) 4907–4911.
[7] T. Ichikawa, H. Fujii, S. Isobe, K. Nabeta, Appl. Phys. Lett. 86 (2005) 1–3, 241914.
[8] R. Ströbel, J. Garche, P.T. Moseley, L. Jörissen, G. Wolf, J. Power Sources 159 (2006) 781–801.
[9] X.B. Yu, Z. Wu, Q.R. Chen, Z.L. Li, B.C. Weng, T.S. Huang, Appl. Phys. Lett. 90 (2007) 1–3, 034106.
[10] J.J. Vajo, S.L. Skeith, F. Mertens, J. Phys. Chem. B 109 (2005) 3719–3722.
[11] I.G. Fernández, G.O. Meyer, F.C. Gennari, J. Alloys Compd. 446/447 (2007) 106–109.
[12] F.C. Gennari, F.J. Castro, J. Alloys Compd. 396 (2005) 182–192.
[13] H.S. Kim, H. Lee, K.S. Han, J.H. Kim, M.S. Song, M.S. Park, J.Y. Lee, J.K. Kang, J. Phys. Chem. B 109 (2005) 8983–8986.
[14] R. Zacharia, S.U. Rather, S.W. Hwang, K.S. Nahm, Chem. Phys. Lett. 434 (2007) 286–291.
[15] F.H. Yang, A.J. Lachawiec Jr., R.T. Yang, J. Phys. Chem. B 110 (2006) 6236–6244.
[16] R. Zacharia, K.Y. Kim, A.K.M.F. Kibria, K.S. Nahm, Chem. Phys. Lett. 412 (2005) 369–375.
[17] E. Yoo, L. Gao, T. Komatsu, N. Yagai, K. Arai, T. Yamazaki, K. Matsuishi, T. Matsumoto, J. Nakamura, J. Phys. Chem. B 108 (2004) 18903–18907.
[18] I. Stamatin, A. Morozan, A. Dumitru, V. Ciupina, G. Prodan, J. Niewolski, H. Figiel, Physica E 37 (2007) 44–48.
[19] S.S. Han, H.S. Kim, K.S. Han, J.Y. Lee, H.M. Lee, J.K. Kang, S.I. Woo, Appl. Phys. Lett. 87 (2005) 1–3, 213113.
[20] S.Y. Kim, H.S. Kim, S. Augustine, J.K. Kang, Appl. Phys. Lett. 89 (2006) 1–3, 253119.
[21] Y. Kojima, N. Suzuki, Appl. Phys. Lett. 84 (2004) 4113–4115.